RESEARCH ARTICLE

CRYSTAL Research & Technology

www.crt-journal.org

Design and Optimization of $C_6H_5NO_2$-Core Photonic Crystal Fibers for Broadband Supercontinuum Generation with Low Peak Power

*Van Trong Dang and Van Lanh Chu**

This study presents a new square-lattice photonic crystal fiber (PCF) with a nitrobenzene core. Considering the non-uniformity of the air hole diameter, this new design allows the characteristic quantities to be optimized simultaneously to ensure near-zero dispersion, a small effective mode area, and low loss for efficient spectral broadening. The spectrum broadens significantly at peak powers many times lower than in previous studies. Based on the obtained results, two optimal PCFs are proposed and validated in detail for supercontinuum generation (SCG). The first fiber #F_1 operates in an all-normal dispersion regime with a pump wavelength of 1.3 µm.It produces a spectral supecontinuum (SC) from 0.726 to 1.649 µm with a pulse duration of 90 fs and a peak power of 133 W. Meanwhile, the second fiber #F_2 operates in anomalous dispersion regime with a pump wavelength of 1.61 µm. With a low peak power of 300 W and a pulse duration of 150 fs, the fiber #F_2 provides SC generation with bandwidth from 0.805 µm to 3.970 µm. The proposed fibers are suitable for all-fiber SC light sources, respectively, and may lead to new low-cost all-fiber optical systems.

1. Introduction

Photonic crystal fibers (PCFs) are a special type of optical fiber that can control the propagation of light.[1] Fabricated based on the properties of photonic crystals with periodic refractive index (RI) distributions in fiber cross-section.[2,3] Unlike conventional fibers, PCF consists of micro-holes running along the fiber axis surrounding a central defect region that serves as the core. According to their structure, PCFs can be classified into index-guiding and photonic band-gap fibers (PBGFs), and all characteristics of PCFs are derived from the presence of air holes in the cladding. PCFs can be used in a variety of research fields and practical applications. Here it is worth mentioning fiber light sources, supercontinuum generation (SCG) devices, fiber optic sensors or nonlinear devices,[2–4] endless single-mode properties,[5] single-polarization single-mode operation,[6] high birefringence,[7,8] tailorable dispersion profiles and flat or ultra-flat dispersion.[9,10] Where the generation of supercontinuum (SC) light is one of the important applications. Because of its unique properties, SCG has been exploited in various prospects including optical coherence tomography, optical metrology, multimodal biophotonic imaging, and high-speed optical communication.[11–14]

The SCG occurs when the ultra-short optical pulses are pumped into a highly nonlinear medium.[15] It is a complex process of spectral broadening of ultra-short optical pulses, which undergo several nonlinear interactions in the optical nonlinear medium. The action of nonlinear effects including Self-Phase Modulation (SPM), Optical Wave Breaking (OWB), Cross-Phase Modulation (XPM), Raman Scattering (SRS), Raman–Kerr Scattering (RKS), Modulation Instability (MI), Soliton Fission (SF), Soliton Self-Frequency Shift (SSFS), and dispersive wave (DW).[16–18] Depending on the choice of the pump wavelength within the dispersion range, the corresponding effects will appear during SCG. Furthermore, to achieve the best SCG efficiency, the PCF should has flat and near to zero dispersion curve, the attenuation and effective mode area should be as small as possible. We can design and tune the structural parameters of PCF such as lattice constant, air-holes size, type of lattices, solid or hollow core, and material to achieve this goal.

A common approach is the development of supercontinuum light sources based on PCFs made of silica or highly nonlinear glasses. Silica is often used in SC generation due to its special purity and very high laser damage threshold. However, Silica is not transparent in the mid-infrared (m-IR) and exhibits relatively low nonlinearity. On the other hand, PCF from highly nonlinear glasses can produce SC generation in the m-IR range. However, a drawback of using soft glass fibers for SCG is their incompatibility with silica-based fiber systems, which are typically performed in expensive and complex experimental systems.[19,20]

Recently, liquid-filled hollow-core fibers have been proposed as an attractive approach for SC generation because liquids exhibit high nonlinearity and high transparency.[19,21–33] **Table 1** gives a brief summary of the results achieved with liquid core PCFs in recent years. Previously reported hollow-core PCFs showed excellent dispersion control and improved nonlinearity, as well as

V. T. Dang, V. L. Chu
Department of Physics
Vinh University, Vinh
Nghe An Province 461010, Vietnam
E-mail: chuvanlanh@vinhuni.edu.vn

The ORCID identification number(s) for the author(s) of this article can be found under https://doi.org/10.1002/crat.202300085

DOI: 10.1002/crat.202300085

Table 1. Overview of SCG in several liquid-core PCFs.

Liquid-Core	Peak power [W]	Pump wavelength [μm]	Fiber length [cm]	SC spectral range [μm]	Regime
CCl_4[27]	62 500	1.03	20	0.85–1.25	All-normal
$CHCl_3$[28]	2500	1.03	10	0.6–1.26	All-normal
$CHCl_3$[28]	2000	1.03	10	0.6–1.4	Anomalous
$C_6H_5NO_2$[22]	1000	1.81	5	1.3–2.8	All-normal
$C_6H_5NO_2$[29]	5550	1.56	5.0	0.8–2.1	All-normal
$C_6H_5NO_2$[29]	660	1.56	5.0	1.3–2.3	Anomalous
C_6H_6[20]	55 000	1.56	1.0	0.7–2.0	All-normal
C_6H_6[20]	37 000	1.56	1.0	0.6–3.5	Anomalous
C_2Cl_4[30]	16 670	1.56	5.0	0.8–2.0	All-normal
C_2Cl_4[30]	16 670	1.56	10	1.0–2.0	Anomalous
C_2Cl_4[30]	20 830	1.03	10	0.7–2.4	Anomalous
$C_2H_4Br_2$[31]	12 500	1.03	10	0.64–1.7	All-normal
$C_2H_4Br_2$[31]	750	1.03	15	0.7–2.4	Anomalous
C_7H_8[32]	7140	1.55	10	1.1–1.75	All-normal
C_7H_8[32]	6670	1.55	10	1.0–1.75	Anomalous
C_7H_8[33]	25 000	1.03	10	0.95–1.1	All-normal
C_7H_8[34]	450	1.064	1	0.642–1.592	All-normal
C_7H_8[34]	550	1.55	10	0.911–2.496	Anomalous

peak performance for generating wide SCs. However, the peak power used by this PCF is very high, up to tens of kW. In most of the works above (Table 1), the diameters of the air holes in the cladding are the same size, so only the dispersion can be optimized in the PCF structure, but not the effective mode area and the attenuation.[27–33]

Most recently, Ref. [34] reported a PCF with a toluene-core (C_7H_8-core) with a circular lattice of SCG. In which, the PCF structure has a difference in air hole diameter between the first ring and the rest of the lattice rings, which helps to optimize the characteristic quantities. However, the authors using a circular lattice PCF structure can only optimize the effective mode area due to its symmetry, but not optimize dispersion. Therefore, the SCG performance of PCF is still limited in this paper.

Nitrobenzene was chosen to fill the hollow-core PCF due to its high nonlinear refractive index of $n_2 = 671 \times 10^{-20}$ m^2 W^{-1} at 1064 nm,[35] which is about 240 times higher than that of Silica,[36] because it is higher than other liquids such as $CHCl_3$, CCl_4, C_2Cl_4, and C_7H_8. Moreover, it has moderate toxicity,[35] relatively low attenuation with respect to other liquids of the nonlinearity, the low vapor pressure at room temperature, and ease of handling.[37] By filling the core with $C_6H_5NO_2$, our previous work on hexagonal lattice PCFs with varying air-holes size showed that the dispersion properties of PCFs can be tuned by achieving flat and low dispersion at peak dispersion wavelengths close to the pump wavelength.[21] This allows optimization of both the effective mode area and attenuation. However, to fully exploit advances in fabrication technology and overcome the limitations of hexagonal PCFs, that is, to enhance the flatness of the spectrum. In this paper, we designed a new square-lattice hollow-core PCF filled with nitrobenzene. The square PCFs play an important role in reaching near-zero ultra-flattened dispersion that contributes to SC generation because it is highly symmetric and easier to design than other types of lattice. An air-filling fraction of square lattice PCF is quite low which causes a higher refractive index of cladding, and hence, the lower field confinement and more interesting dispersive characteristics. A series of numerical simulations are performed to investigate the effects of initial pulse characteristics (input peak power and pulse duration) on the SC bandwidths of the two optimal structures, achieving wider bandwidths than previous work with low-peak power.

The article is structured as follows. Part 2 describes the numerically constructed $C_6H_5NO_2$ core PCF. The next section discusses optimizing the PCF parameters. In Section 4, we show that the optimally selected low-peak power fiber achieves an extended spectrum with high efficiency compared to previous studies. Finally, Section 5 presents the conclusion of the work.

2. Numerical Modeling

A study on the chromatic dispersion of solid-core PCFs by Saitoh et al.[38] showed that the lattice parameter of the air hole near the core has a significant effect on the dispersion properties of the PCFs, comprising the normal or anomalous regime, zero-dispersion wavelength shift (ZDW), flat dispersion characteristic. The second ring onward is mainly responsible for attenuation, especially higher-order modes, and bending conditions. In this work, the authors did not apply the obtained results to SCG but analyzed only the PCF features. Based on this idea, we designed a PCF structure in which the diameter of the air holes in the first lattice ring is different from the other lattice rings.

The PCF consists of eight rings of air holes with diameter d, arranged in a square lattice with lattice constant Λ, as shown in **Figure 1**. A finite-difference eigenmode (FDE) method with an anisotropic perfectly matched layer (PML) was used to obtain important properties such as dispersion coefficients, effective mode

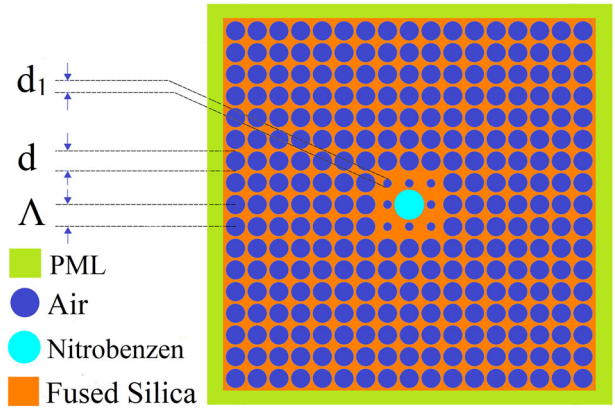

Figure 1. The geometrical structure of PCF in our work.

areas, and nonlinear coefficients. In PCFs, changing the air-hole size and lattice constant can significantly change all optical parameters, but the physical realization remains a real challenge. The linear filling factor of the photonic cladding is determined by the formula $f = d/\Lambda$. Control the filling factor d_1/Λ to optimize dispersion characteristics (d_1 is the air-hole diameter of the first lattice ring near the core) and set the filling factor in the remaining lattice rings (d/Λ) to 0.95 to optimize the effective mode area and loss. The lattice constants (Λ) chosen for the study varied from 1.0 to 2.5 μm with a step of 0.5 μm and the filling factor d_1/Λ was varied from 0.3 to 0.8 with a step size of 0.05. The PCF structure is simulated over a limited wavelength range of 0.5 to 2.0 μm, as data are probably only available in this wavelength range. The diameter of the core satisfies the formula $D_c = 2\Lambda - 1.1d_1$, where D_c is the diameter of the core. The maximum core diameter is $D_{cmax} = 4.175$ μm corresponding to the case $\Lambda = 2.5$ μm and $d_1/\Lambda = 0.3$ and the minimum core diameter value is $D_{cmin} = 1.12$ corresponds to $\Lambda = 1.0$ μm and $d_1/\Lambda = 0.8$. This size range takes into account the limitations of the stack-and-draw process commonly used to manufacture PCF.[39] Either a fusion splicer or a laser scribing technique is used to selectively introduce the liquid into the core of the PCF.[40,36] Liquid is filled into the PCF core based on an integrated microfluidic pumping system. These analyzes apply only to optimal fibers and do not guarantee whether the PCF chosen is single-mode or multi-mode.

Figure 2a shows the real part characteristics of the wavelength refractive index of $C_6H_5NO_2$ compared with that of fused silica. It can be seen that the refractive index of $C_6H_5NO_2$ is always greater than that of SiO_2. Therefore, the light transmitted in PCF based on Silica with a $C_6H_5NO_2$-core follows the same total internal reflection mechanism as in conventional optical fibers. On the other hand, On the other hand, we experimentally measure the imaginary part k of the linear refractive index, as shown in Figure 2b.

The real part of the linear refractive index n of $C_6H_5NO_2$ and SiO_2 is calculated as a function of wavelength using the Sellmeier formula in Equations (1) and (2).[41,42]

$$n^2_{Nitrobenzene}(\lambda) = 1 + \frac{1.30628\lambda^2}{\lambda^2 - 0.02268} + \frac{0.00502\lambda^2}{\lambda^2 - 0.28487} \quad (1)$$

$$n^2_{Silica}(\lambda) = 1 + \frac{0.6694226\lambda^2}{\lambda^2 - 4.4801.10^{-3}} + \frac{0.4345839\lambda^2}{\lambda^2 - 1.3285.10^{-2}} + \frac{0.8716947\lambda^2}{\lambda^2 - 95.341482} \quad (2)$$

Dispersion in an optical fiber includes a waveguide dispersion and material dispersion according to the formula Equation (3), where Re[n_{eff}] is the real part of the effective refractive index of the guided mode and c is the speed of light in a vacuum.[43]

$$D = -\frac{\lambda}{c}\frac{\partial^2 \mathrm{Re}[n_{eff}]}{\partial \lambda^2} \quad (3)$$

The units of the nonlinear coefficients of the PCF are ($W^{-1}\,km^{-1}$), determined by the formula in Equation (4).[43]

$$\gamma(\lambda) = 2\pi\frac{n_2}{\lambda A_{eff}} \quad (4)$$

where A_{eff} is the effective mode area (an important feature of PCF). It is inversely proportional to the nonlinear coefficient and is given by Equation (5).[43]

$$A_{eff} = \frac{\left(\int_{-\infty}^{\infty}\int_{-\infty}^{\infty}|E|^2 dxdy\right)^2}{\int_{-\infty}^{\infty}\int_{-\infty}^{\infty}|E|^4 dxdy} \quad (5)$$

where E is the electric field amplitude.

The PCF properties are computed based on "a full-vector finite difference mode solver."[44] This solver divides the cross-section of the fiber into small rectangular sections called "Yee's mesh." The optical properties of each Yee mesh are approximated as unchanged. For points lying on the surface between two media, an index averaging technique is used for the cells across the interface. Note that optimization algorithms are not used in this document, but better optical properties can be obtained with optimization algorithms. It can be explained that the structural parameters of PCFs vary very slightly, consistent with a "stack-and-draw" manufacturing process of about 50 nm (For example, the filling factor varies by 0.05, and the lattice constant changes by 0.5 μm).[39] Moreover, using optimization algorithms during simulation takes a lot of time. Therefore, a simpler method based on the optimization of dispersion properties was applied.

3. Optimization of the Characteristic Quantities of PCF

Figure 3 shows the effect of varying the filling factor (d_1/Λ) and the lattice constant (Λ) on the dispersion (D). Looking at the diagram, we can see that the square lattice structure has varying dispersion at different wavelengths. The resulting dispersion curves contain all-normal and anomalous dispersions with one or two ZWDs. The dispersion properties were governed by changing the filling factor d_1/Λ and the lattice constant (Λ). Moreover, changing these two parameters shifts the ZDW to longer wavelengths.

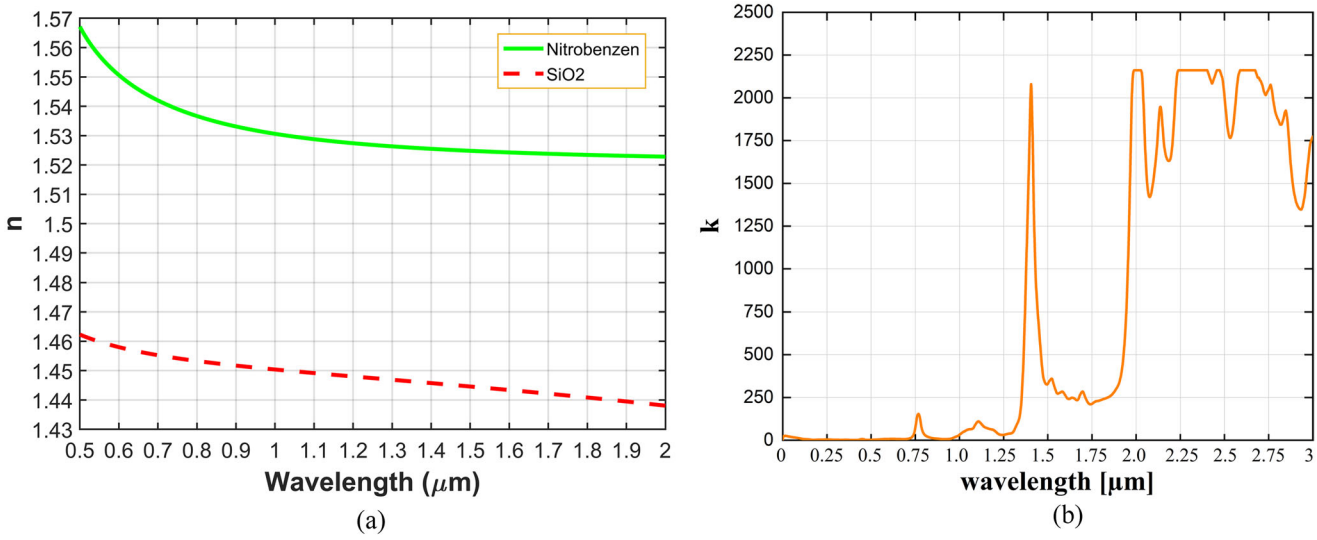

Figure 2. a) Real parts of the refractive index of $C_6H_5NO_2$ and SiO_2. b) The imaginary part of the refractive index k of $C_6H_5NO_2$.

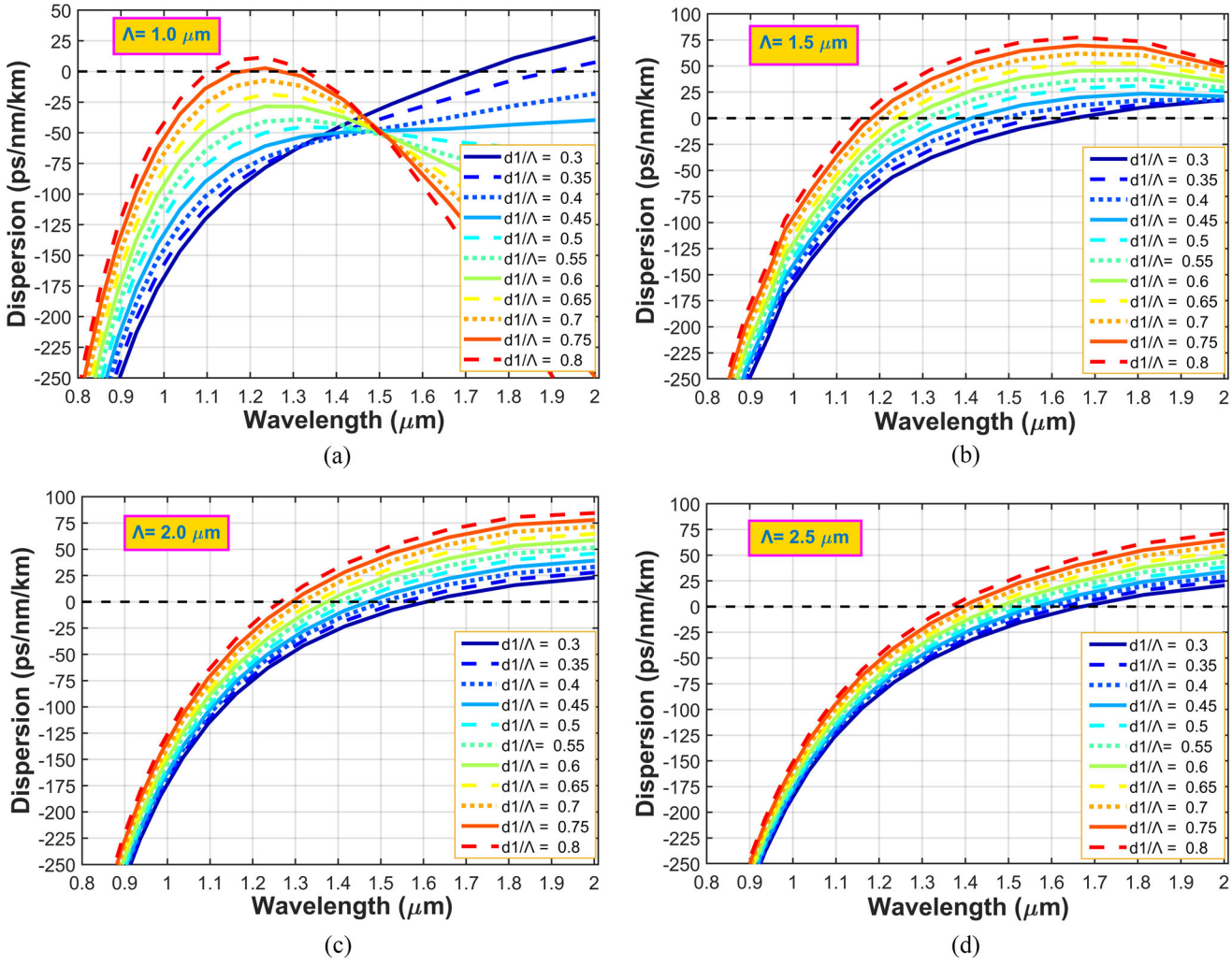

Figure 3. The dispersion properties of $C_6H_5NO_2$-core PCFs have different Λ with values of d_1/Λ varying from 0.3 to 0.8. a) $\Lambda = 1.0$ μm, b) $\Lambda = 1.5$ μm, c) $\Lambda = 2.0$ μm, and d) $\Lambda = 2.5$ μm.

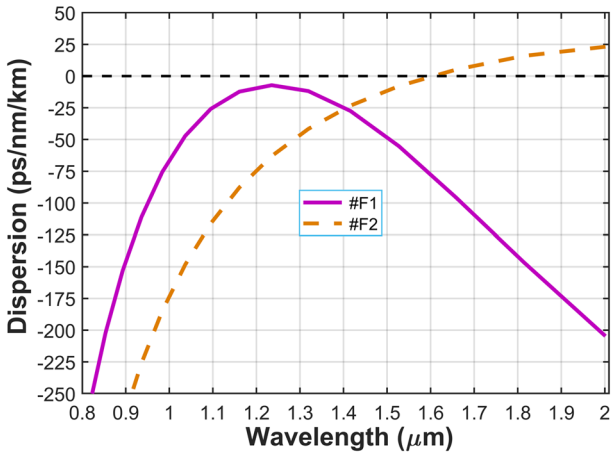

Figure 4. The chromatic dispersion of the selected structures.

At small lattice parameters ($\Lambda = 1.0$ μm, Figure 3a), PCFs exhibit both anomalous and normal dispersion properties. A PCF with two ZDWs values can be obtained for $d_1/\Lambda = 0.75$ and $d_1/\Lambda = 0.8$, whereas the PCF only yields one ZDW with $d_1/\Lambda \leq 0.35$ in the examined wavelength range. In this case, all-normal dispersion usually occurs only when $0.4 \leq d_1/\Lambda \leq 0.7$. This fiber has flat dispersion and is close to the zero dispersion curve in the long wavelength range, which is expected to be useful for the SC generation. On the other hand, all PCFs with larger cores ($\Lambda = 1.5$ μm, $\Lambda = 2.0$ μm, $\Lambda = 2.5$ μm) are in the anomalous dispersion regime with one ZDW. Moreover, for a given value of Λ ($\Lambda >$ 1.0 μm), the ZDW shifts to longer wavelengths as the filling factor d_1/Λ decreases. In contrast, for some values of filling factor d_1/Λ, the ZDW shifts to shorter wavelengths as the Λ deceases. The above analysis and simulation results show that by carefully tuning the air hole diameter d_1 of the first ring of the PCF structure, it seems that the desired dispersion properties of the structure can be easily obtained.

The optimal structure chosen for SCG should have a flat dispersion curve and be close to the zero-dispersion curve. Based on this, we selected two optimal fibers for SCG, namely #F_1 ($d_1/\Lambda = 0.7$; $\Lambda = 1.0$ μm) and #F_2 ($d_1/\Lambda = 0.3$; $\Lambda = 2.5$ μm. **Figure 4** shows the dispersion properties of the proposed fiber. Fibers #F_1 operate in an all-normal dispersion regime, with a maximum dispersion value of −7.208 ps nm^{-1} km^{-1} located at a wavelength of 1.235 μm. SC generation using PCF with an all-normal dispersion regime has a great advantage in the output pulses are coherent, high stability, and flat, making any work effort possible. The pump wavelength for the fiber #F_1 is chosen to be 1.3 μm. This is because this value is close to the wavelength value at the maximum point of the dispersion curve. This makes it possible for the fiber to obtain an extended spectrum. On the other hand, the fiber #F_2 exhibits anomalous dispersion and has a zero-dispersion wavelength at 1.607 μm. Therefore, we chose a pump wavelength of 1.61 μm for the fiber #F_2 (the pump wavelength chosen here satisfies the condition of having a larger value and being close to the zero-dispersion wavelength). The dispersions of fibers #F_1 and #F_2 at the pump wavelength are −10.764 and 0.319 ps nm^{-1} km^{-1}, respectively.

Figure 5a shows the fundamental mode attenuation characteristics of fibers #F_1 and #F_2. Attenuation of the proposed fibers include confinement loss and material loss of $C_6H_5NO_2$ in the core as well as silica in the cladding. Since $C_6H_5NO_2$ has higher refractive index than silica, the light is strongly confined inside the core resulting in low confinement loss. Consequently, attenuation profiles of fibers with various core diameters follow the material attenuation of $C_6H_5NO_2$, see Figure 5a. However, in the mid-IR range, a fiber with a small core diameter (#F_1: D_{core} = 1.23 μm) has a attenuation slightly higher than a large core fiber (#F_2: D_{core} = 4.175 μm). The higher attenuation of the small core fiber originates from confinement and high absorption of silica in the mid-IR range. The attenuation of fiber #F_2 is the smallest and almost coincides with the horizontal axis. The attenuation value at 1.3 μm pump wavelength for fiber #F_1 is 0.271 dB cm^{-1}. A low attenuation is an advantage of our model compared to previous studies. The effective mode area of the proposed PCF is shown in Figure 5b. The results in the figure show that the effective mode area for both fibers increases linearly with increasing wavelength. Due to the larger core diameter, the effective mode area for #F_2 is always larger than the case of others. At the pump wavelength, fibers #F_1 and #F_2 have effective mode area values of 1.462 (μm^2) and 6.978 (μm^2), respectively. The nonlinear coefficient is inversely proportional to the effective mode area according to Equation (4), so it tends to decrease linearly with increasing wavelength, Figure 5c. The nonlinearity of fiber #F_1 is always larger than that of #F_2, the nonlinearity value of the former is 2107 (W^{-1} km^{-1}) at the pump wavelength, while that of #F_2 is 441 (W^{-1} km^{-1}). **Table 2** shows a comparison between the proposed fiber properties and previously published values. The two proposed fibers of this work have many times smaller attenuation compared to the works compared in Table 2.[21,27,30,32,33] In the normal dispersion regime, the fiber #F_1 has a smaller effective mode area than previously reported, leading to higher nonlinear coefficients.[21,27,30,32,33] In this case, the nonlinear coefficients of the fiber #F_1 are 95 times and 13 times larger than that of the previous Ref. [27] and Ref. [28]. Moreover, for the anomalous dispersion regime, the effective mode area values in our study are much smaller than those in the compared studies.[27,30,32,33]

4. Supercontinuum Generation in Optimized PCFs

The nonlinear propagation process of the pump pulse in the PCF can be expressed in terms of the Schrödinger equation (GNLSE) using the symmetric split-step Fourier transform method,[43] which is given by the formula:

$$\partial_z \tilde{A} - i\tilde{\beta}(\omega)\tilde{A} - \frac{\tilde{\alpha}(\omega)}{2}\tilde{A} = i\gamma\left(1 + \frac{\omega - \omega_0}{\omega_0}\right)\tilde{A}F\left[\int_{-\infty}^{\infty} R(T')|A|^2(T - T')\,dT'\right] \quad (6)$$

where $\tilde{A}(\omega)$ is the Fourier transform of the amplitude of the pulse $A(t)$.

On the left side of Equation (6), the linear parameters α and β represent propagation loss and dispersion in the frequency domain of an optical fiber. Higher-order dispersion shows a

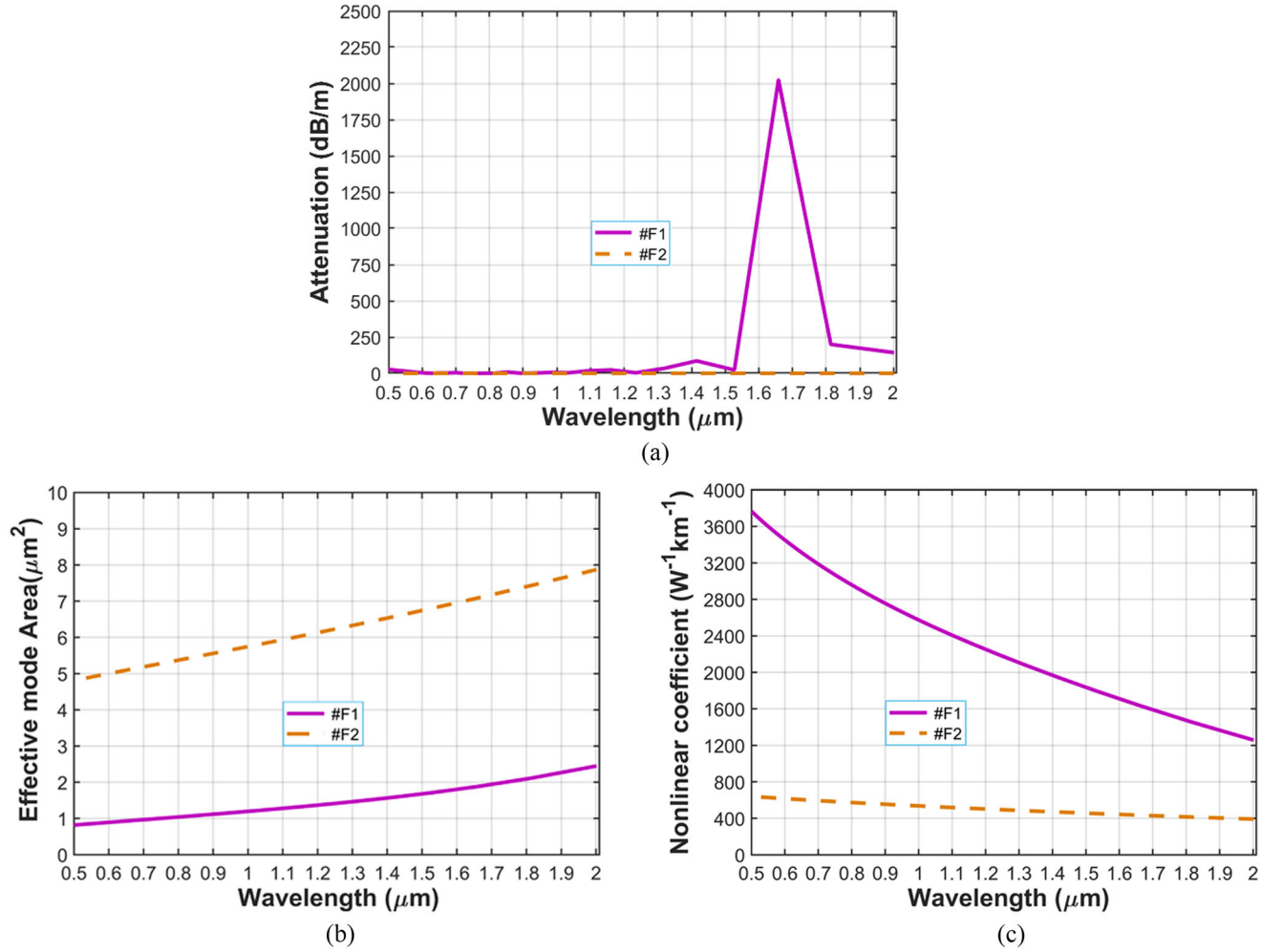

Figure 5. a) The attenuation of the fundamental mode for fiber #F_1 and #F_2, b) the effective mode area of the fundamental mode for fiber #F_1 and #F_2, and c) the nonlinear coefficient of the fundamental mode for fiber #F_1 and #F_2.

Table 2. The characteristic values of the proposed PCFs in comparison with previous publications.

#	Pump wavelength [μm]	D [ps nm^{-1} km^{-1}]	A_{eff} [μm^2]	γ [km^{-1} W^{-1}]	Attenuation [dB cm^{-1}]	Regime
#F_1 [This work]	1.3	−10.764	1.462	2107	0.271	All-normal
#F_2 [This work]	1.61	0.319	6.978	441	6×10^{-17}	Anomalous
$C_6H_5NO_2$, #HF_1[21]	1.56	−3.18	2.059	1.496	6.52	All-normal
$C_6H_5NO_2$, #HF_2[21]	1.55	6.215	6.538	471	4.92	Anomalous
CCl_4[27]	1.03	−85	42.2	22.1	-	All-normal
C_2Cl_4, #F_1[30]	1.56	−15.0	433.2	156.9	0.04	All-normal
C_2Cl_4, #F_2[30]	1.56	3.20	16.67	40.79	0.042	Anomalous
C_2Cl_4, #F_3[30]	1.03	−4.85	359.1	189.3	0.053	Anomalous
C_7H_8, #I_0.3[32]	1.55	−7.784	7.79	1200	0.4	All-normal
C_7H_8, #I_0.35[32]	1.55	−1.19	78.9	-	1.2	Anomalous
C_7H_8[33]	1.03	−150 ÷ −5	73.2	130	-	All-normal

Table 3. The coefficients of high-order chromatic dispersion at the pump wavelength.

Coefficient	#F_1	#F_2
β_2 (ps^2/m)	9.23×10^{-3}	-1.01×10^{-3}
β_3 (ps^3/m)	-8.32×10^{-5}	1.21×10^{-4}
β_4 (ps^4/m)	1.26×10^{-6}	-3.96×10^{-7}
β_5 (ps^5/m)	-4.28×10^{-9}	1.78×10^{-8}
β_6 (ps^6/m)	-1.95×10^{-12}	-4.93×10^{-12}
β_7 (ps^7/m)	-1.20×10^{-12}	-4.66×10^{-12}
β_8 (ps^8/m)	2.44×10^{-14}	2.48×10^{-14}
β_9 (ps^9/m)	4.63×10^{-16}	9.50×10^{-16}
β_{10} (ps^{10}/m)	-1.72×10^{-17}	-9.58×10^{-18}
β_{11} (ps^{11}/m)	-4.97×10^{-20}	-1.92×10^{-19}

significant effect as the center wavelength of the input pulse approaches the ZDW and is calculated by the expansion coefficients of the Taylor series around the center wavelength ω_0, the expansion of the propagation constant (β) can be obtained by[40]

$$\beta_k(\omega) = \left.\frac{d^k \beta(\omega)}{d\omega^k}\right|_{\omega=\omega_0} \tag{7}$$

where $k = 2, 3, 4$ are the dispersion coefficients. **Table 3** shows the higher-order dispersion at the pump pulse frequency in numerical modeling.

The right-hand side of the equation depicts the nonlinear effects which depend on the nonlinear optical response of nitrobenzene that is identified by the combination of the bound-electronic and nuclear contribution. The subscripts *el*, *d*, *l*, and *c* indicate the bound-electronic, molecular reorientation, molecular interaction, and collision induced, respectively. τ_r and τ_f are rise time and fall time. The Raman response function $R(t)$ is described in Equation (8):

$$R(t) = \left(1 - f_R\right)\delta(t) + f_R R(t') \tag{8}$$

where $\delta(t)$ is the Dirac delta function and f_R is a part of the delayed contribution, which is a fraction of nuclear contribution to the nonlinear optical response of nitrobenzene. f_R of nitrobenzene is ≈0.87.

$R(t')$ represents the delayed nonlinear response, is a sum of the electronic-bound and molecular contribution mechanisms which is able to be defined as in the following Equation (9):[45]

$$R\left(t'\right) = \frac{1}{N}\left[2n_{el} + \left(n_{2l}C_{21}e^{-t/t_{fl}}\int_0^\infty \frac{\sin\left(\omega t'\right)}{\omega} g(\omega)\, d\omega + \sum_{k=c,d} n_{2k}C_{2k}\left(1 - e^{-t'/t_{rk}}\right)\Theta\left(t'\right)\right)\right] \tag{9}$$

where $N = n_{2el} + n_{2c} + n_{2d} + n_{2l}$, and the values of $n_{2,el}, n_{2,d}, \tau_{r,d}, \tau_{f,d}, n_{2,l}, n_{2,c}, \tau_{r,c}, \tau_{f,c}, \tau_{f,l}$ are determined as follows:

$$\begin{aligned} &n_{2,el} = 0.6 \times 10^{-19}\mathrm{m}^2/\mathrm{W}; \quad n_{2,d} = 5.0 \times 10^{-19}\mathrm{m}^2/\mathrm{W}; \\ &n_{2,l} = 1.7 \times 10^{-19}\mathrm{m}^2/\mathrm{W}; \quad n_{2,c} = 0.35 \times 10^{-19}\mathrm{m}^2/\mathrm{W}; \\ &\tau_{r,d} = 0.1\mathrm{ps}, \quad \tau_{f,d} = 3.5\mathrm{ps}, \quad \tau_{r,c} = 0.2\mathrm{ps}, \\ &\tau_{f,c} = 0.1\mathrm{ps}, \quad \tau_{f,l} = 0.4\mathrm{ps} \end{aligned} \tag{10}$$

The laser pulses used in the simulation is modeled by a Gaussian pulse centered at the pump wavelength with P_0 as the peak power and t_0 as pulse duration given by Equation (11).[46]

$$A(T) = \sqrt{P_0}\exp\left(\frac{-T^2}{2t_0^2}\right) \tag{11}$$

SC generation in the two proposed fibers was studied with different pulse parameters. For the fiber #F_1, the SC generation in the all-normal dispersion regime is pumped at 1.3 μm, with a pulse duration of 90 fs, and the peak varying from 22 to 133 W. The fiber #F_1 has a pulse propagation length of 1 cm. The fiber #F_2 was analyzed with a ZDW of 1.607 μm wavelength, SC generation at peak powers ranging from 7 W to 300 kW, a propagation length of 15 cm, a pump wavelength of 1.61 μm, and a pulse duration of 150 fs.

Figure 6 shows the temporal and spectral evolution of the pulse over a propagation distance of 1 cm at various peak powers in the fiber #F_1. Since #F_1 has a pump pulse that operates with an all-normal dispersion, the SC generation process is dominated by two main effects, namely SPM and OWB. Looking at Figure 6a, we can see that the spectral width increases as the peak power increases. For low peak power fibers of 22 and 44 W, SPM makes the greatest contribution to spectral broadening. This results in a finitely conserved spectrum and a spectrum composed of many peaks, with the peaks having the greatest intensity. When the peak power is greater than 44 W, the SC spectrum is determined by the SPM in the early stages of propagation and the resulting spectrum is asymmetric for short wavelengths due to the effect of nonlinear dispersion. Subsequently, the emergence of OWB generated by four-wave mixing (FWM) was the dominant effect in spectral broadening in these cases. The OWB begins to appear at 67 W peak power at 0.88 μm and helps the spectrum broaden rapidly as the peak power continues to increase. OWB appears at shorter wavelengths. At a peak power of 133 W, the spectrum broadens from 0.726 to 1.649 μm with a relative power range of 5 dB. Figure 6b shows the temporal structure at different positions of the propagation length with the spectrum growing along the fiber #F_1. In general, the higher the input peak power, the faster the time delay between different frequencies and the shorter the propagation. Considering both cases, these values increase with increasing distance due to different group velocity components.

For fiber #F_2, SC generation was analyzed at a pump wavelength of 1.61 μm, a pulse width of 150 fs, and a fiber propagation length of 15 cm. Fiber #F_2 has a pump wavelength within the anomalous dispersion regime, so soliton dynamics, for example, SF, SSFS, play an important role in spectral broadening. As the process propagates further, the solitons continue to shift to longer wavelengths, resulting in a very large extension of the received spectrum toward the red-light region. Moreover, the DW

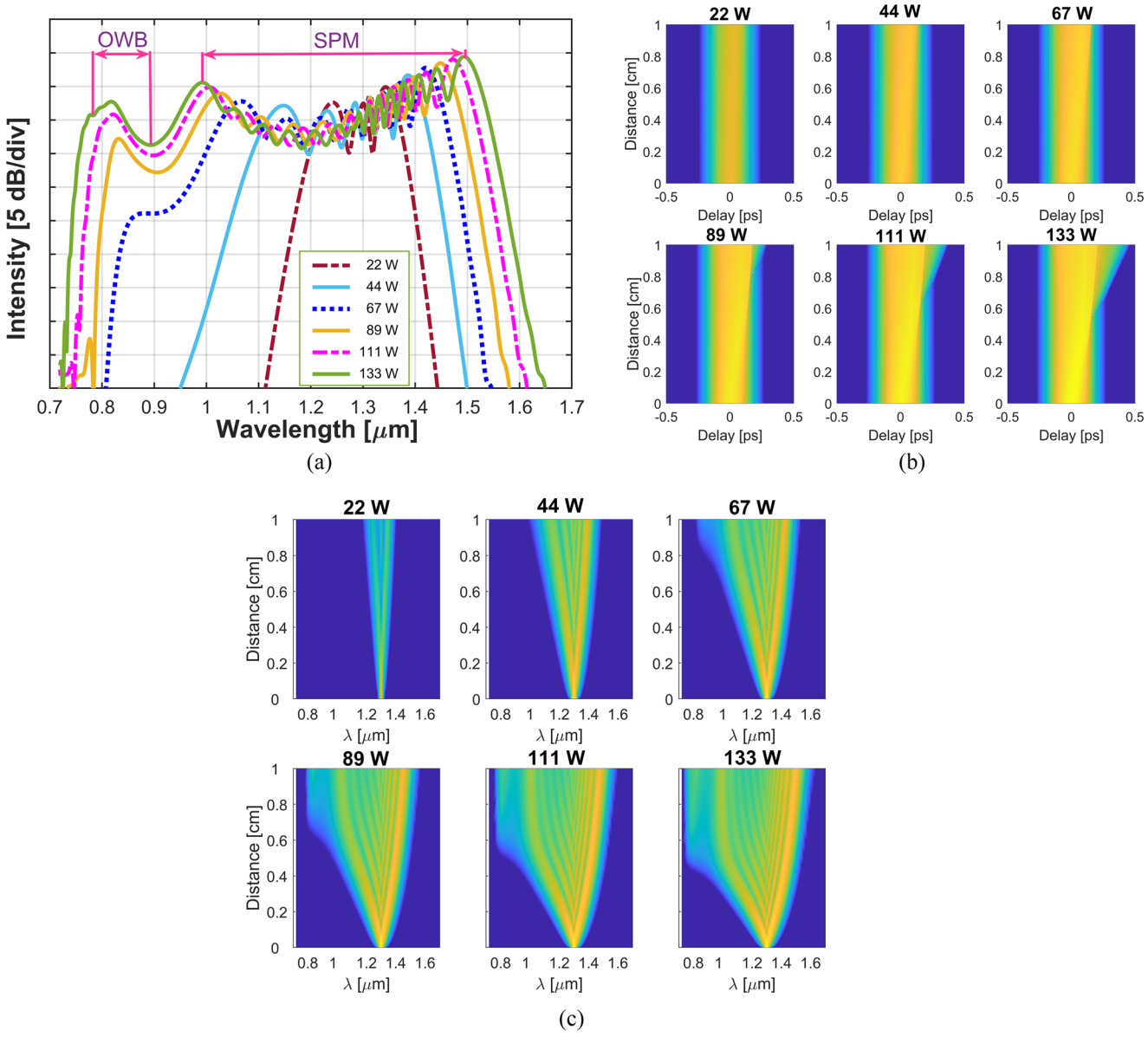

Figure 6. For fiber #F_1: a) the output spectrum for various peak power pulses when using pump pulses with 1.3 μm pump wavelength and 90 fs duration, b) the temporal profile at various propagation lengths, and c) the pulse evolution of the SC along with fiber.

component is generated by four-wave mixing and propagates without frequency shift.

Figure 7 shows the spectral broadening at different peak powers. At a peak power of 7 W, the SPM plays a major role in spectral broadening, so the resulting spectrum is smaller in this case. Beyond a peak power of 7 W, soliton fission begins to appear, broadening the spectrum. As peak power increases, spectral width increases. However, when the peak power is 300 W, the spectral width is almost the same as when the peak power is 267 W. This is explained by factors such as high dispersion slope in the short wavelength range, low nonlinear coefficient and high loss in the long wavelength range. When the peak power equals 300 W, the spectral bandwidth expands from 0.805 to 3.970 μm with a dynamic range of 10 dB.

We find that the SCG performance of our project is more optimal than that shown in Table 1. Especially for the anomalous dispersion region, the SC spectra obtained in our study have the lowest peak power and the broadest compared to the studies in Table 1. In the all-normal dispersion regime, our proposed fiber can achieve the same bandwidth as the comparative claims but uses much lower peak power. In particular, the fiber #F_1 has an extended spectrum from 0.726 to 1.649 μm with a peak power of 133 W, while the fiber in Ref. [31] has an extended spectrum from 0.64 to 1.7 μm but uses 93 times more peak power than our work. PCF with an all-normal dispersion regime in Ref. [20] used a peak power of 55 000 W and is 413 times larger than our work, but the obtained spectral band is approximately equal to that of our fiber #F_1. Moreover, the spectral range of our PCFs in all-normal

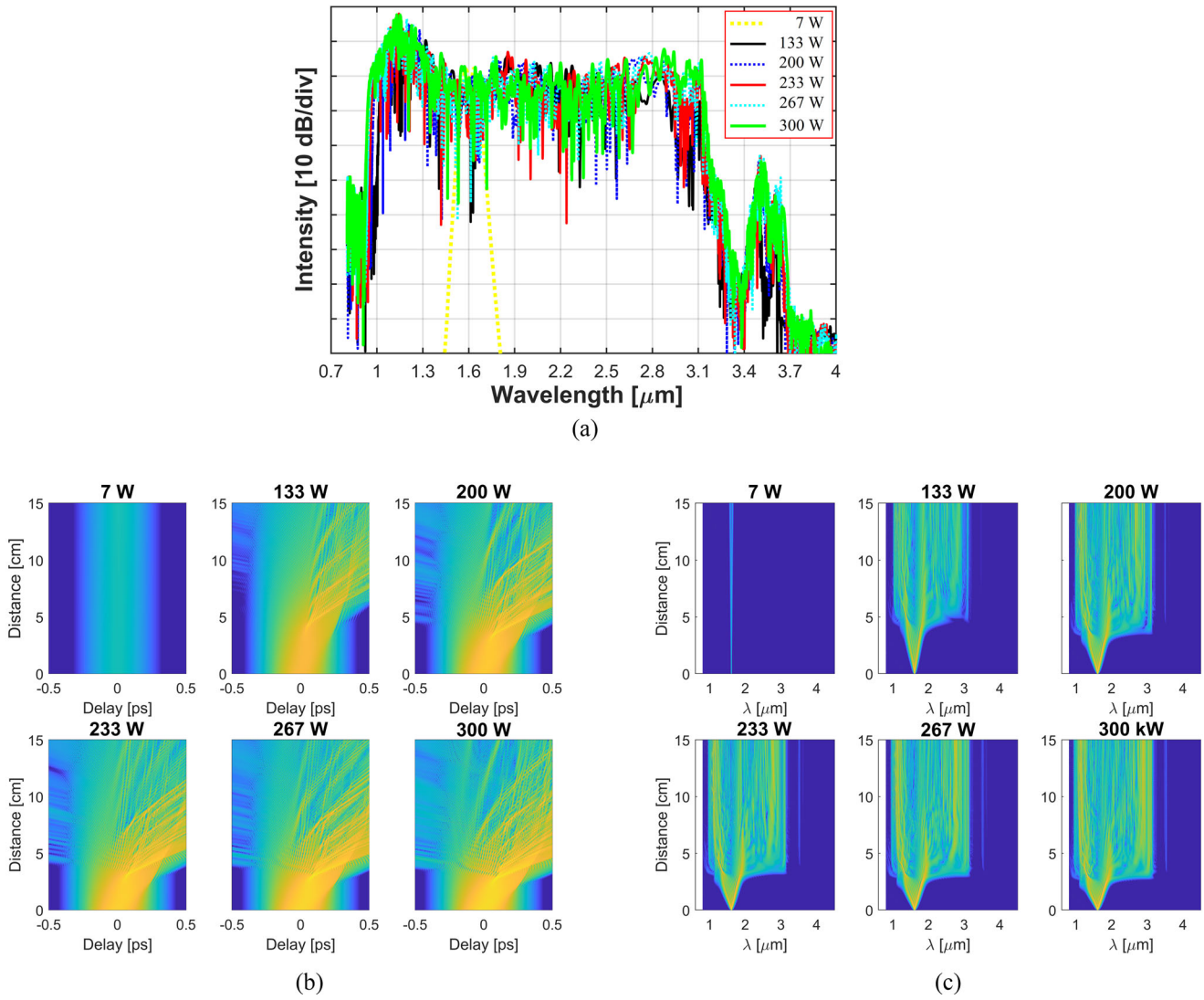

Figure 7. For fiber #F_2:a) the output spectrum for various peak power pulses when using pump pulses with 1.61 μm pump wavelength and 150 fs duration, b) the temporal profile at various propagation lengths, and c) the pulse evolution of the SC along with the fiber.

dispersion is larger than that of the C_7H_8-filled PCFs in the previous study,[32,33] but the peak power used is lower. The all-normal dispersion fiber in Ref. [34] has a structure with varying air hole diameter, as in our work, we obtained a spectral band approximately equal to that of #F_1 in this work, but using a peak power three times larger. The above results demonstrate the high potential of the proposed PCF for coherent and broad SC generation systems.

5. Conclusion

In this article, we have improved the dispersion and nonlinear properties of $C_6H_5NO_2$-infiltrated square-lattice PCFs by making the size of the air holes in the innermost layer different from the other air holes. The numerical analysis proposes two optimal structures are proposed with flat and small dispersion, which are highly suitable for SC generation. At the same time, the nonlinear properties of the optimal fiber including small effective mode area, high nonlinear coefficient, and low attenuation, also show their impact on SC spectral quality. The square lattice optimized PCF (fiber #F_1) with all-normal dispersion, a small value of −10.764 ps nm^{-1} km^{-1} was obtained at a pump wavelength of 1.3 μm. The flat dispersion and a small effective mode area of 1.462 $μm^2$ contribute to a wide spectral range from 0.726 to 1.649 μm with a low peak power of 133 W for ultra-short pulses propagating in a 1 cm length fiber. On the other hand, the SC spectrum with anomalous dispersion is much broader than that of PCFs with all-normal dispersion. Fiber #F_2 has a rather small dispersion of 0.319 ps nm^{-1} km^{-1} a nonlinear coefficient of 441 W^{-1} km^{-1} and approximately zero attenuation in the wavelength range investigated. A wide spectral range of 0.805 to 3.970 μm is achieved with a peak power of 300 W and a duration of 150 fs when #F_2 is pumped at 1.61 μm, propagating in a 15 cm long fiber. We expect the low-cost compact all-fiber SC system based on the proposed fibers to be further expanded in future practical applications.

Acknowledgements

Dang Van Trong was funded by the Master, PhD Scholarship Programme of Vingroup Innovation Foundation (VINIF), code [VINIF.2022.TS136].

Conflict of Interest

The authors declare no conflict of interest

Data Availability Statement

Research data are not shared.

Keywords

dispersion, nitrobenzene core, photonic crystal fiber, square lattice, supercontinuum generation

Received: April 11, 2023
Revised: June 8, 2023
Published online:

[1] J. C. Knight, T. A. Birks, P. S. J. Russell, D. M. Atkin, *Opt. Lett.* **1996**, *21*, 154.
[2] J. C. Knight, *Nature* **2003**, *424*, 847.
[3] P. S. J. Russell, *Science* **2003**, *299*, 358.
[4] R. Buczynski, *Acta Phys. Pol. A* **2004**, *106*, 141.
[5] T. A. Birks, J. C. Knight, P. S. J. Russell, *Opt. Lett.* **1997**, *22*, 961.
[6] Z. Hui, D. Hou, Y. Zhang, S. Wei, J. Xu, *Fiber Integr. Opt.* **2019**, *38*, 91.
[7] A. Bala, K. R. Chowdhury, M. B. Mia, M. Faisal, *Appl. Opt.* **2017**, *56*, 7256.
[8] C. V. Lanh, B. T. L. Tran, T. D. Van, V. T. M. Ngoc, T. N. Thi, N. T. H. Phuong, T. N. M. Hang, V. T. Hoang, *Opt. Fiber Technol.* **2023**, *75*, 103151.
[9] J. Lægsgaard, P. J. Roberts, M. Bache, *Opt. Quantum Electron.* **2007**, *39*, 995.
[10] J. M. Hsu, *Opt. Commun.* **2016**, *361*, 104.
[11] M. Guillon, K. Dholakia, D. McGloin, *Opt. Express* **2008**, *16*, 7655.
[12] H. Tu, S. A. Boppart, *Laser Photonics Rev.* **2013**, *7*, 628.
[13] W. J. Ling, K. Li, Y. Y. Zuo, *App. Mech. Mater.* **2013**, *302*, 194.
[14] H. Liu, Y. Yu, W. Song, Q. Jiang, F. Pang, *Opto-Electron. Adv.* **2019**, *2*, 180020.
[15] J. M. Dudley, G. Genty, S. Coen, *Rev. Mod. Phys.* **2006**, *78*, 1135.
[16] L. C. Van, L. M. Van, Q. H. Quang, *Commun. Phys.* **2008**, *18*, 255.
[17] L. C. Van, L. M. Van, K. D. Xuan, S. V. Ngoc, T. N. T. Thanh, Q. H. Quang, *Commun. Phys.* **2008**, *18*, 119.
[18] C. V. Lanh, D. X. Khoa, *Commun. Phys.* **2007**, *17*, 227.
[19] C. V. Lanh, T. N. Thi, D. H. Trong, B. T. L. Tran, V. T. M. Ngoc, T. D. Van, L. C. Trung, Q. D. Ho, D. Q. Khoa, *Opt. Quantum Electron.* **2022**, *54*, 300.
[20] L. C. Van, V. T. Hoang, V. C. Long, K. Borzycki, K. D. Xuan, V. T. Quoc, M. Trippenbach, R. Buczynski, J. Pniewski, *Opt. Eng.* **2021**, *60*, 11.
[21] T. D. Van, L. C. Van, *Mod. Phys. Lett. B* **2023**, https://doi.org/10.1142/S021798492350063X
[22] J. Wen, B. Liang, W. Qin, W. Sun, C. He, K. Xiong, *Opt. Quantum Electron.* **2022**, *54*, 817.
[23] V. Devika, M. S. M. Rajan, M. Sharma, *Opt. Quantum Electron.* **2022**, *54*,858.
[24] V. Devika, M. S. M. Rajan, H. Thenmozhi, A. Sharafali, *J. Opt.* **2022**, *52*, 539.
[25] S. Kedenburg, A. Steinmann, R. Hegenbarth, T. Steinle, H. Giessen, *Appl. Phys. B* **2014**, *117*, 803.
[26] H. Takahashi, I. Sugimoto, T. Takabayashi, S. Yoshida, *Opt. Commun.* **1985**, *53*, 164.
[27] V. T. Hoang, R. Kasztelanic, A. Filipkowski, G. Stępniewski, D. Pysz, M. Klimczak, S. Ertman, V. C. Long, T. R. Wolin´ski, M. Trippenbach, K. D. Xuan, M. Śmietana, R. Buczyński, *Opt. Mater. Express* **2019**, *9*, 2264.
[28] L. C. Van, T. V. Hoang, V. C. Long, K. Borzycki, K. D. Xuan, V. T. Quoc, M. Trippenbach, R. Buczyński, J. Pniewski, *Laser Phys.* **2019**, *29*, 075107.
[29] L. C. Van, T. V. Hoang, V. C. Long, K. Borzycki, K. D. Xuan, V. T. Quoc, M. Trippenbach, R. Buczyński, J. Pniewski, *Laser Phys.* **2020**, *30*, 035105.
[30] H. V. Le, V. T. Hoang, H. T. Nguyen, V. C. Long, R. Buczynski, R. Kasztelanic, *Opt. Quantum Electron.* **2021**, *53*, 187.
[31] H. V. Le, V. T. Hoang, Q. D. Ho, H. T. Nguyen, N. V. T. Minh, M. Klimxzak, R. Buczynski, R. Kasztelanic, *Appl. Opt.* **2021**, *60*, 7268.
[32] L. C. Van, A. Anuszkiewicz, A. Ramaniuk, R. Kasztelanic, K. D. Xuan, V. C. Long, M. Trippenbach, R. Buczynski, *J. Opt.* **2017**, *19*, 125604.
[33] V. T. Hoang, R. Kasztelanic, A. Anuszkiewicz, G. Stepniewski, A. Filipkowski, S. Ertman, D. Pysz, T. Wolinski, K. D. Xuan, M. Klimczak, R. Buczynski, *Opt. Mater. Express* **2018**, *8*, 3568.
[34] T. N. Thi, D. H. Trong, B. T. L. Tran, T. D. Van, L. C. Van, *J. Opt.* **2022**, *51*, 678.
[35] Y. Xu, X. Chen, Y. Zhu, *Sensors* **2008**, *8*, 1872.
[36] M. Vieweg, T. Gissibl, S. Pricking, B. T. Kuhlmey, D. C. Wu, B. J. Eggleton, H. Giessen, *Opt. Express.* **2010**, *18*, 25232.
[37] R. L. Sutherland, D. G. McLean, S. Kirkpatrick, *Handbook of Nonlinear Optics*, CRC Press, Boca Raton, **2003**.
[38] K. Saitoh, M. Koshiba, T. Hasegawa, E. Sasaoka, *Opt. Express.* **2023**, *11*, 843.
[39] D. Pysz, I. Kujawa, R. Stępień, M. Klimczak, A. Filipkowski, M. Franczyk, L. Kociszewski, J. Buźniak, K. Haraśny, R. Buczyński, *Bull. Pol. Acad. Sci. Tech. Sci.* **2014**, *62*, 667.
[40] L. Xiao, W. Jin, M. Demokan, H. Ho, Y. Hoo, C. Zhao, *Opt. Express.* **2005**, *13*, 9014.
[41] S. Kedenburg, M. Vieweg, T. Gissibl, H. Giessen, *Opt. Mater. Express* **2012**, *2*, 1588.
[42] C. Z. Tan, *J. Non-Cryst. Solids* **1998**, *223*, 158.
[43] G. P. Agrawal, *Nonlinear Fiber Optics*, Academic Press, Elsevier, Cambridge **2013**.
[44] Z. Zhu, T. G. Brown, *Opt. Express.* **2002**, *10*, 853.
[45] H. Zhang, S. Chang, J. Yuan, D. Huang, *Optik* **2010**, *121*, 783.
[46] F. Koohi-Kamalia, M. Ebnali-Heidarib, M. K. Moravvej-Farshic, *Int. J. Opt. Phot. (IJOP)* **2012**, 6, 83.